Vietnam Journal of Earth Sciences, 41(4), 358–373, Doi: 10.15625/0866-7187/41/4/14237

(VAST)

Vietnam Academy of Science and Technology

Vietnam Journal of Earth Sciences

http://www.vjs.ac.vn/index.php/jse

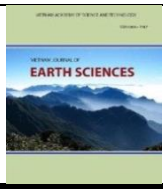

Spatial distribution of submerged aquatic vegetation in An Chan coastal waters, Phu Yen province using the PlanetScope satellite image

Nguyen Thi Thu Hang[1], Nguyen Thai Hoa [2], Nguyen Van Tu[3], Nguyen Ngoc Lam[4*]

[1]*Graduate University of Science and Technology, VAST, Hanoi, Vietnam*
[2]*Department of Natural Resources and Environment of Phu Yen province, Vietnam*
[3]*Institute of Tropical Biology, VAST, Hanoi, Vietnam*
[4]*Institute of Oceanography, VAST, Hanoi, Vietnam*

Received 24 May 2019; Received in revised form 18 August 2019; Accepted 1 September 2019

ABSTRACT

Seaweed and seagrass form marine submerged aquatic vegetation (SAV), which plays an essential role in economic development and ecological protection in coastal areas. In this study, PlanetScope (PS)imaging data was combined with in situ samplings to demonstrate their ability to map SAV distribution in An Chan commune, Tuy An district, Phu Yen province, Central Vietnam. Thanks to data pre-processing by Lyzenga's algorithm and the masking in PS image allow us to remove partly the signals of spectral noises from sun glint effect as well as other random noises. The analysis and accuracy assessment of SAV classification by four different techniques: DII, enhanced DII, BRI and enhanced BRI were alternately performed. The overall accuracy in the accuracy assessment of SAV classification by the above techniques were alternately 83.33%, 88.58%, 86.17%, and 92.52% respectively. Kappa coefficients in the accuracy assessment of SAV classification by the above techniques were alternately 0.77, 0.84, 0.81 and 0.90 respectively. The results of SAV classification by enhanced BRI technique provided the best accuracies and will be chosen for assessing the distribution of Submerge Aquatic Vegetation (SAV) canopies in An Chan coastal waters from PS satellite image. The seagrass beds in An Chan is spread along the coast as well as lie close to the coast of islets. Whereas, the seaweed meadows lie in deeper waters and in the foot of the reefs in 3–4m deep. The total seagrass area in An Chan region was approximately 12.22 ha, with 10.93 ha seagrasses in My Quang, 1.18 ha in Hon Chua and 0.11 ha in Hon Dua. The total seaweed area in An Chan region was approximately 50.32 ha, with 20.20 ha seaweed meadows in My Quang, 22.8 ha in Hon Chua, 5.72 ha in Hon Dua and a small part of 1.60 ha in underwater small reefs.

Keywords: PlanetScope satellite image; seagrass; seaweed; SAV mapping; DII; BRI.

1. Introduction

Remote sensing technology has significantly been supporting the observation of the Earth's surface. The advantages of this technique include wide monitoring, repetitive, observation, low cost and not requiring a majority of manpower (Chauvaud et al., 1998); Brown et al., 2011). The multi-spectral or hyper-spectral images with high spatial resolution assists scientist to precisely detect different patterns on the Earth (Mumby,

*Corresponding author, Email: ngoclam-ion@planktonviet.org.vn

1999), (Larkum et al., 2006). Today, orbit spectral images expand its scale to the underwater ecosystem and effectively create aquatic resource maps (Green et al., 1996). In the field of mapping of submerging aquatic vegetation canopies, water column correction is the driving factor that improves the accuracy of habitat mapping. There were three main approaches in water column correction according to different algorithm groups: (i) Band combination algorithms; (ii) Model-based quasi-analytic algorithms; and (iii) Spectrum matching ones. The approach of algorithms related to the first group is relatively simple that base on the analyzing "image to image" and assume that bottom radiance in any band in the visual light domain is an exponential function of depth and attenuation coefficient in that band. Given that depth in a pixel is constant for all bands, the algorithms in this group attempt to linearize the relation between radiance in each band pair, namely Depth Invariance Index-DII technique (Lyzenga, 1981; Spitzer and Dirks, 1987; Conger et al., 2006; Pu et al., 2012, Siregar et al., 2016; Chen et al., 2016; Pu and Bell, 2017, Gašparović et al., 2018) and/or establish exponential relationship between radiance/reflectance and water depth, namely Bottom Reflectance Index-BRI technique (Sagawa et al., 2010, Hashim et al., 2014; Koedsin et al., 2016). Algorithms in second group regarding to quasi-analytic models require measurements on the optical properties in water medium (include the Inherence Optical Properties-IOP and Appearance Optical Properties-AOP) with more complex calculations for estimating the spectral signal in sea surface and seabed (Bierwirth et al., 1993; Purkis and Pasterkamp, 2004; Mumby et al., 1998; Yang et al., 2010). This data has just obtained will be an important information source for marine habitat mapping with improved accuracy. However, algorithms in this group only were used well for quasi-ocean color data that contain many spectral bands (more than four bands) and include the short wave infrared-SWIR ones. Algorithms in the third group regarding optimize spectrum matching models. They simulating the spectra for different water column characteristics and mapping the spectra similarities with the simulated spectral library (Lee et al., 2002; Mobley et al., 2005; Klonowski et al., 2007; Brando et al., 2009; Hedley et al., 2009). The result is a substrate map independent of the water column effect. Hyperspectral data provides information almost continuous in the visible light domain that can be able to distinguish more detail between submerged substrates base on the algorithms in the third group. However, the generation of a giant spectral library requires actual bottom reflectance measured in situ. For this reason, all types of substrate reflectance in all possible combinations occurring in the scene must be accurately represented. In order to map underwater habitats with orbit multi-spectral images (as PlanetScope satellite image in this study), the approach of combination band algorithms is most appropriate. Moreover, both DII and BRI methods applied very well for underwater habitat mapping and biomass estimating (such as coral reef, seagrass beds,…) in shallow water, but they met certain errors when detecting of seaweed meadow in deeper waters. Tassan proposes a new concept on the differentiation of the attenuation coefficients in shallow water where is higher brightness and in deeper waters where is lower brightness (Tassan, 1996). Hassan's algorithm is a modified DII (and BRI as well) method through numerical simulations for application in environments with important gradients in turbidity between shallow and deep waters and improves the processed results by discrimination the attenuation coefficients between two shallow/deeper water zones.

In this paper by mean of application the different band combination algorithms, the authors attempt to detect the distribution of submerging aquatic vegetation canopies in coastal waters of An Chan-Phu Yen province

by PlanetScope image. Four main indies (include DII-Depth Invariant Index (Lyzenga, 1981), BRI-Bottom Reflectance Index (Sagawa, 2010) and their improved indies according to Tassan's concept on un-homogeneous of attenuation coefficient along vertical profile of water column (Tassan et al., 1996) will be sequentially analyzed and detected the submerge vegetation canopies in An Chan-Hon Chua coastal waters. The classification results of submerging substrates in the studied area then were compared quantifiable in terms of the accuracy to propose the best technique for marine habitat mapping in An Chan-Hon Chua coastal waters by PlanetScope image.

2. Material and methodologies

2.1. Object and research scope

Our objects are seagrass and seaweed canopies at coastal waters in My Quang – Hon Chua, An Chan commune Tuy An District, Phu Yen province, Vietnam (Fig. 1). This is open coastal waters have enormous potential for developing tourism and a marine-based economy. It is also an area with high biodiversity and many rare and precious species such as turtles, squid, lobsters and sea cucumbers have been recorded (Phu Yen DONRE, 2014). In periods when waterline reaches the lowest level, the tidal flat in a fishing village in North My Quang exposed in the air with the vast seagrass beds with 1000 m long and 320 m wide. The brown seaweed meadows of *Sargassum* spp. In this region usually, grow most strongly in April-June every year. The seagrass beds and *Sargassum* seaweed meadows in My Quang-Hon Chua are targeted to be detected from PlanetScope images in this paper.

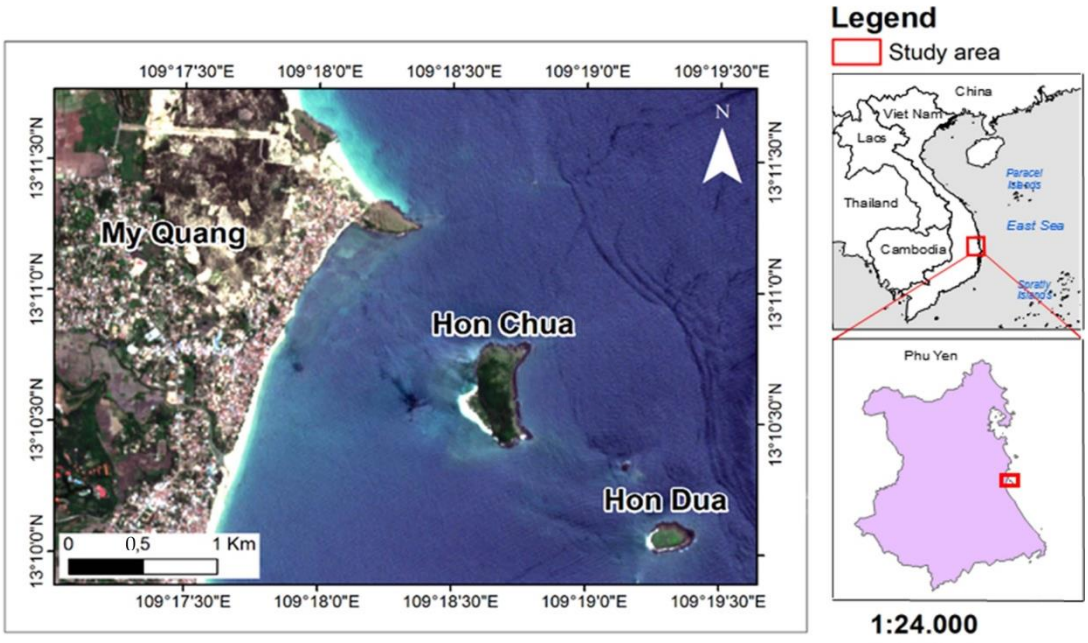

Figure 1. Map of pilot study area, An Chan commune, Phu Yen province, central Vietnam

2.2. Data and methodology

2.2.1. Satellite image

Two image scenes of PlanetScope, level 1B, the acquisition time of 28 June 2018 with the code number of 20180628_024114_1004 and 20180628_024115_1004 have been ordered from PlanetScope constellation

belong to European Space Agency (ESA). PlanetScope (PS) image has the spatial resolution of 3,1 m*3,9 m with 4 spectral bands in the visible spectral bands: Blue (455–515 nm), Green (550–590 nm), Red (590–670nm), and NIR (780–680 nm). PlanetScope scenes that use in this study get radiometric resolution of 16 bit (i.e 216 = 65536 spectral differentiation in each pixel). This scene was already geo-corrected by ESA in Geographic Long/Lat Projection, Datum WGS84 and then have been resampled into the projection of UTM, Datum WGS84, Zone 49, in spatial resolution 5m*5m. The covered scope of two Planetscope image scenes that were used in this study show in Fig. 2.

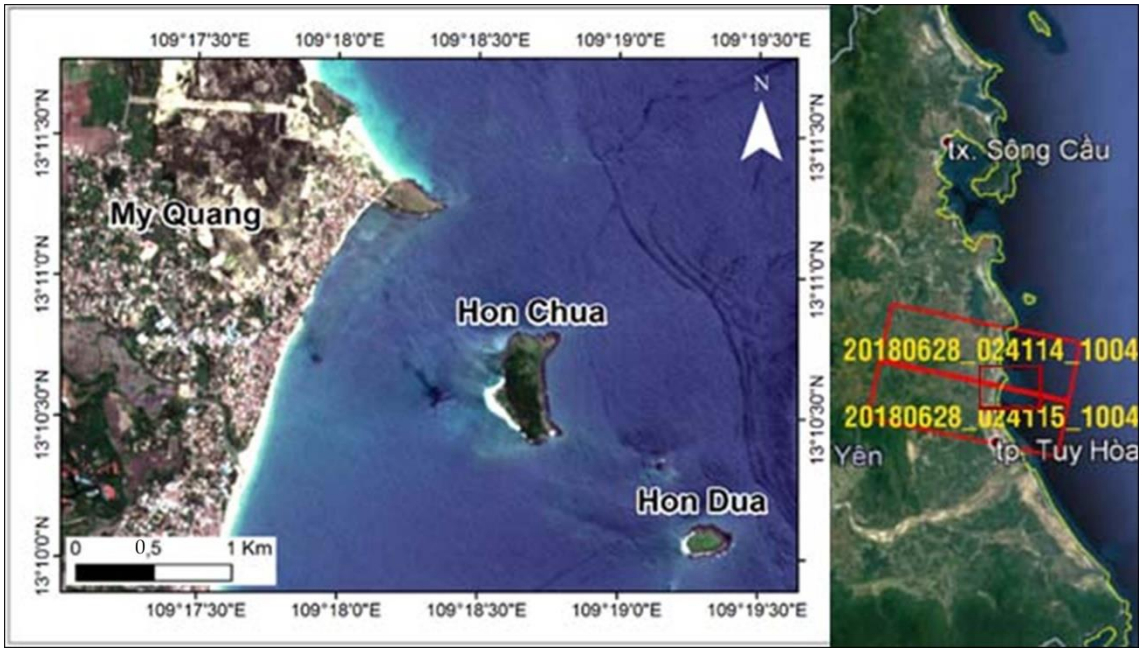

Figure 2. The covered scope of two PlanetScope image scenes were used in this study

2.2.2. Field survey and bathymetry data

Point survey and quadrat method were conducted at coastal shallow waters (include both areas of My Quang tidal flat when low tide) to set up the essential keys for the detection of distribution of submerged aquatic vegetation (SAV) and other bottom substrates in coastal waters of An Chan. We utilized the ship and boats to sample the seagrass, seaweed and observe the distribution of SAV and other habitats in shallow waters of An Chan commune. Moreover, the sampling of SAV and others also were carried out along cross-sections in My Quang tidal flat when low tide by walking. More than 700 GPS points (marked by Garmin Oregon 450) were recorded to locate the SAV canopies and different habitats from the survey in June 2018. Coverage, fresh biomass, and species classification are essential inputs. In addition, we observed fresh sand beds in Xep beach where lie in Northside of My Quang, and perform to sample in the points with a homogeneous sand bed along 3 adjacent cross-sections from shore to 15 m depth. This data of sand points will be used for analyzed DII as well as BRI that will be presented in the next parts. SAV samples after collection were washed, soaked in 5% formol solution and transferred to the laboratory of Marine Plant Division, Nha Trang Institute of Oceanography for analyzing. Taxonomic

literature such as Philips and Menez (1988), Ho Pham Hoang (1969), Tsutsui et al. (2005) and Tien (2013) were used to identify the species of SAV. Species names were updated by http://www.algaebase.org

Depth point data were obtained from in situ measurements by echo-sounder instrument Lawrance VP 1000 in coastal waters of An Chan-Yen Cape at June 2018. A small scene of Phu Yen bathymetry map that covers An Chan coastal waters will be cropped equivalently to covering the frame of the mosaic image that obtains from two above PlanetScope ones (Fig. 3). Then, processing of rasterizing and resampling to convert the bathymetry map into An Chan depth image with a spatial resolution of 5 m * 5 m. This thing allows to overlap depth data into spectral data that are obtained from PS image, and then easily apply them for analyzing DII, BRI,… as will be discussed more detail in the next sections.

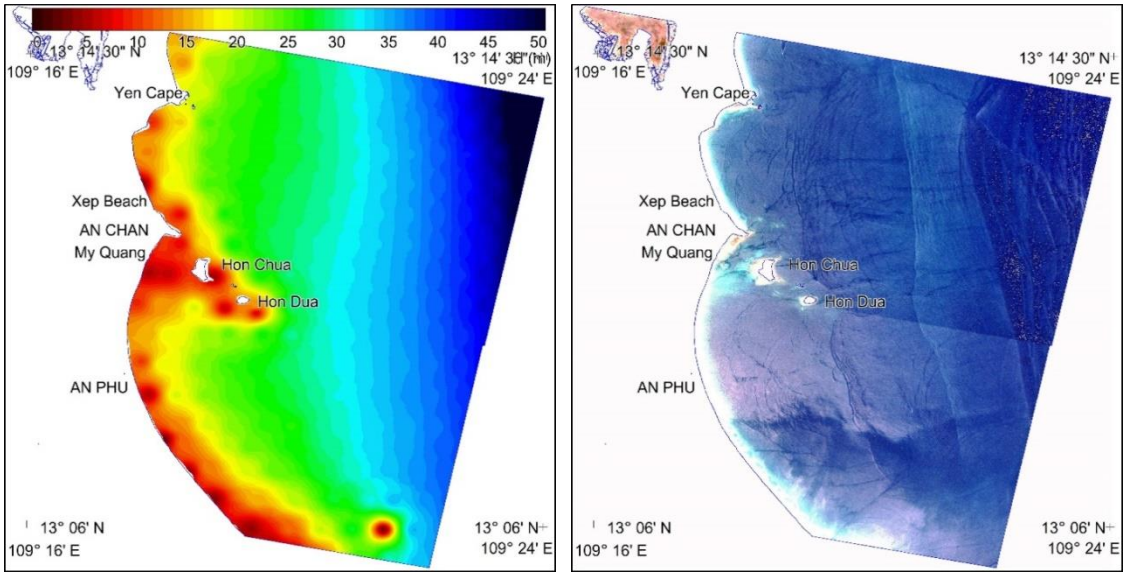

Figure 3. Ref_TOA image in An Chan coastal shallow waters

2.2.3. PlanetScope data processing for detection the distribution of SAV canopies

The distribution of SAV canopies in An Chan coastal waters will be assessed by remote sensing techniques base on PlanetScope (PS) image source. All applied algorithms for extracting SAV canopies in this study require data that have been geometrically corrected, radiometrically calibrated and masked for land and clouds, as well as removed solar glint (if available). Most of them also require previous atmospheric correction. And then, the water column correction, the most important step in detection procedure SAV will be performed. Four band combination algorithms related to water column correction will be applied, compared the accuracy by confusion matrixes and determined the best technique for extracting the distribution of SAV canopies and other substrates in An Chan coastal waters.

PlanetScope (PS) imageries, level 1B that use in this study were already geo-corrected and atmospherically corrected into Reflectance in Top of Atmospheric (Ref_{TOA}). In practice, we only apply a multiple factors of 0.0001 for all of four original DN bands of PlanetScope image and then creating the Ref_{TOA} image. The noise of solar glint appeared in Ref_{TOA} PS image, a procedure of removing the solar glint will be carried by

Lyzenga's algorithm (Lyzenga et al., 2006). This procedure will be performed step by step as following: Isolate a deep water area where get strong signals of sun glint. Then, calculating the covariance (ρ_{ij}) and variance (ρ_{jj}) between visible bands (bands i) and the near-infrared (NIR band-Band j). And next, divide the covariance (ρ_{ij}) into the variance (ρ_{jj}). And the final step, using r_{ij} as the slope of least squares regression curve between visible bands and NIR band for removing the effects of sun glint

$$L_i' = L_i - r_{ij}(L_j - \overline{L_j}) \quad (1a)$$

$$\text{with } r_{ij} = \frac{\rho_{ij}}{\rho_{jj}} \text{ and}$$

$$\rho_{ij} = \frac{1}{N}\sum_{n=1}^{N} L_{in}.L_{jn} - \frac{1}{N}\sum_{n=1}^{N} L_{in} * \frac{1}{N}\sum_{n=1}^{N} L_{jn} \quad (1b)$$

$\overline{L_J}$ is average reflectance of NIR band in deep waters where the signal of sun glint appears clearly.

In the next step, we applied continuously atmospheric correction by Dark Subtract tool for removing atmospheric noises in the optical deep water area and creating a new image of (Ref_{TOA} - $Ref_{TOA,\infty}$). Anh then, the step of water column correction with four different algorithms will be performed. They include algorithm of Lyzenga's DII, Tassan's modified DII, Sagawa's BRI and modified BRI ones.

Lyzenga's algorithm mathematically described the relationship between the bottom reflectance and radiance values which recorded at satellite sensor (Lyzenga, 1981). The $DII_{i,j}$ of each band pair were showed by formula as following

$$DII_{i,j} = Ln\left(Ref_{TOA,i} - Ref_{TOA,\infty,i}\right) - \left[Kd_{i,j}.\left(Ln\left(Ref_{TOA,j} - Ref_{TOA,\infty,j}\right)\right)\right] \quad (2)$$

$Kd_{i,j.}$ corresponds to a proxy of the attenuation coefficient of band pair i and j. They were extracted from the slope of the regression in plot natural logarithms of the band i versus band j that run along homogenous sand bed pixels in different depths.

Tassan's algorithm (Tassan, 1996) was a modifying of Lyzenga's one through numerical simulations for application in environments with important gradients in turbidity between shallow and deep waters, and was represented by double formula.

$$\begin{cases} DII_{i,j} = Ln\left(Ref_{TOA,i} - Ref_{TOA,\infty,i}\right) - \left[Kd_{i,j(LowAlbedo)}.\left(Ln\left(Ref_{TOA,j} - Ref_{TOA,\infty,j}\right)\right)\right] \text{ in upper water layer} & (2a) \\ DII_{i,j} = Ln\left(Ref_{TOA,i} - Ref_{TOA,\infty,i}\right) - \left[Kd_{i,j(HighAlbedo)}.\left(Ln\left(Ref_{TOA,j} - Ref_{TOA,\infty,j}\right)\right)\right] \text{ in lower water layer} & (2b) \end{cases}$$

Sagawa and his colleagues (Sagawa et al., 2010) developed an index to estimate bottom reflectance based on Lyzenga's method (Lyzenga, 1981). Depth data of various pixels on a homogeneous substrate (sand) allowed estimation of the attenuation coefficient Kdi. They corresponded to the constancy of exponential regression line of radiance in band i according to various Z depths, respectively. The bottom reflectance index (BRI) of Sagawa's algorithm was represented by formula as follows.

$$BRI_i = \frac{Ln\left(Ref_{TOA,i} - Ref_{TOA,\infty,i}\right)}{e^{Kd.Z}} \quad (3)$$

The fourth algorithm that will be analyzed in this study, in fact, is a modifying of Sagawa's one with the attention of Tassan's concept on the differentiation of light attenuation between shallow and deep waters. Modified BRI algorithm was represented by double formula.

$$\begin{cases} BRI_{i,HighAlbedo}^{Modify} = \dfrac{Ln\left(Ref_{TOA,i} - Ref_{TOA,\infty,i}\right)}{e^{Kd_{HighAlbedo}.Z}} & \text{in upper water layer} \quad (4a) \\ BRI_{i,LowAlbedo}^{Modify} = \dfrac{Ln\left(Ref_{TOA,i} - Ref_{TOA,\infty,i}\right)}{e^{Kd_{LowAlbedo}.Z}} & \text{in lower water layer} \quad (4b) \end{cases}$$

All of four techniques as above mention will be utilized in various pixels along 3 adjacent cross-sections from shore to 15 m depth in Xep Beach where existed a

homogeneous sand bed. The spectral information of (Ref_{TOA}-$Ref_{TOA,\infty}$) between band pairs or between (Ref_{TOA}-$Ref_{TOA,\infty}$) and the depth are important data for estimating the DII or BRI.

2.2.4. Accuracy assessment (Congalton, 1991)

Confusion matrix was used to evaluate the accuracy of classification results by remote sensing techniques, using the following formula:

$$K = \frac{N\sum_{i=1}^{r} x_{ii} - \sum_{i=1}^{r}(x_{i+} \cdot x_{+i})}{N^2 - \sum_{i=1}^{r}(x_{i+} \cdot x_{+i})} \quad (5)$$

where N: total number of sampling pixels,

r: number of class objects,

x_{ii}: the number of pixels that are correct in i layer,

x_{i+}: total pixels in i layer of the sample,

x_{+i}: total pixels in i layer of the sample after classification.

The kappa coefficient is usually between 0 and 1, and for values within this range, the accuracy of the classification is acceptable. Kappa (Ƙ) has three value groups:

Ƙ> 0.8 : high precision

0.4 <Ƙ <0.8 : moderate accuracy

Ƙ <0.4 : low accuracy

3. Results and discussions

3.1. SAV species composition

3.1.1. Seaweed species composition

Samples of seaweed were collected during three field trips. Seventy-two seaweed species were identified, belonging to four Phyla: Cyanobacteria, Chlorophyta, Ochrophyta, and Rhodophyta. The species composition of Rhodophyta was the most diverse, with 30 species, accounting for 41.67% of the total number of species. Chlorophyta followed with 21 species, accounting for 29.17%, then Ochrophyta with 16 species, accounting for 22.22%, and the least diverse was the Cyanobacteria, with five species, accounting for 6.94% of the total number of species. One species of seaweed was listed in the Red Book of Vietnam: *Hydropuntia eucheumatoides* (Vietnam Red Book, 2007).

Study on the density and distribution of seaweeds in An Chan commune showed that Hon Chua island had the highest species diversity and density (51 species), followed by My Quang (41 species) and then Hon Dua island (24 species). In My Quang area, the species composition and density of Chlorophyta were higher than those in Hon Chua and Hon Dua. However, in this study, we only focus to detect the brown *Sargassum* seaweed meadows that develop strongly at June 2018 in An Chan coastal waters.

3.1.2. Seagrass species composition

In the field surveys in An Chan commune, Tuy An district, Phu Yen province, four seagrass species were identified: *Thalassia hemprichii, Cymodocea rotundata, Halodule uninervis* and *Halophila ovalis. T. hemprichii* was the dominant species with the highest density, followed by *C. rotundata* and *H. uninervis. Halophila* ovalis was scattered among the seagrass beds. In fact, in this study, we only interst to detect the distribution mono- specie seagrass beds of broad leaf *Thalassia hemprichii* in My Quang, Hon Chua and Hon Dua.

3.2. Removing the noises from solar glint and others

By mean of application Lyzenga's algorithm (Lyzenga et al., 2006) for removing the solar glint in mosaic PS image, big patches of sun glitter have been avoided from PS Ref_TOA image (Fig. 4). In additional, spectral signals of underwater substrates (such as sea-grasses, seaweed meadows, sand beds,…) will be showed more clearly and easier to distinguish more and more by visual interpretation (also see Fig. 4-right). Attentional that, after image pre-processing of the removing the signals of sun glitter, we only remain 3 visual bands (i.e R, G, B bands), whereas NIR band absolutely disappear from PS image for next analyzing steps.

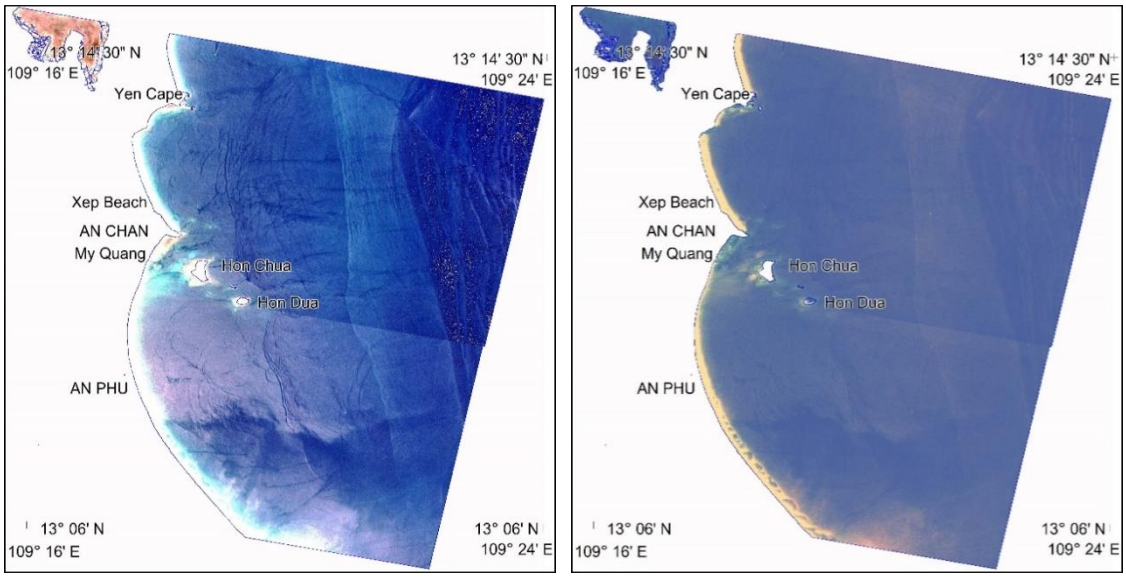

Figure 4. Removing the solar glint before (left) and after (right) of PS mosaic image

The masking both the land as well as surrounding water parts, allowed us to enhance not only visual interpretation but also to remove spectral noises that cause more errors in digital classification process in next step (Fig. 5).

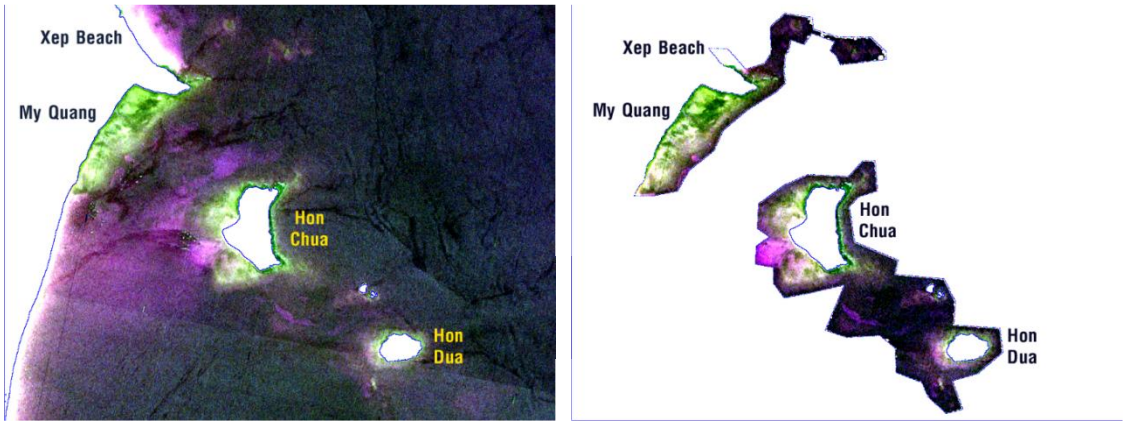

Figure 5. The masking of the land (left) and the masking both the land plus surrounding waters (right)

3.3. SAV Mapping from PS images

3.3.1. Determining the datasets of attenuation coefficients and processing equation systems of the Depth Invariance Indies (DIIs (Fig. 6) and the Bottom Reflectance Indies (BRIs) (Fig. 7)

Through of the observing homogenous sand beds in Xep Beach and surrounding shallow waters, we chose sandy pixels along 3 adjacent cross sections from shore of Xep Beach to 15 m depth. Thanks for good overlapping between spectral image (Ref_TOA) and bathymetry one, allow us to determine simultaneously attenuation coefficients of both DII and BRI algorithms as well as their enhancements. Base on visual observing along plot of Ref_TOA_i versus depth (Fig. 6, right/outside; Fig 7), we determined more concretely attenuation coefficients in each case, as follows.

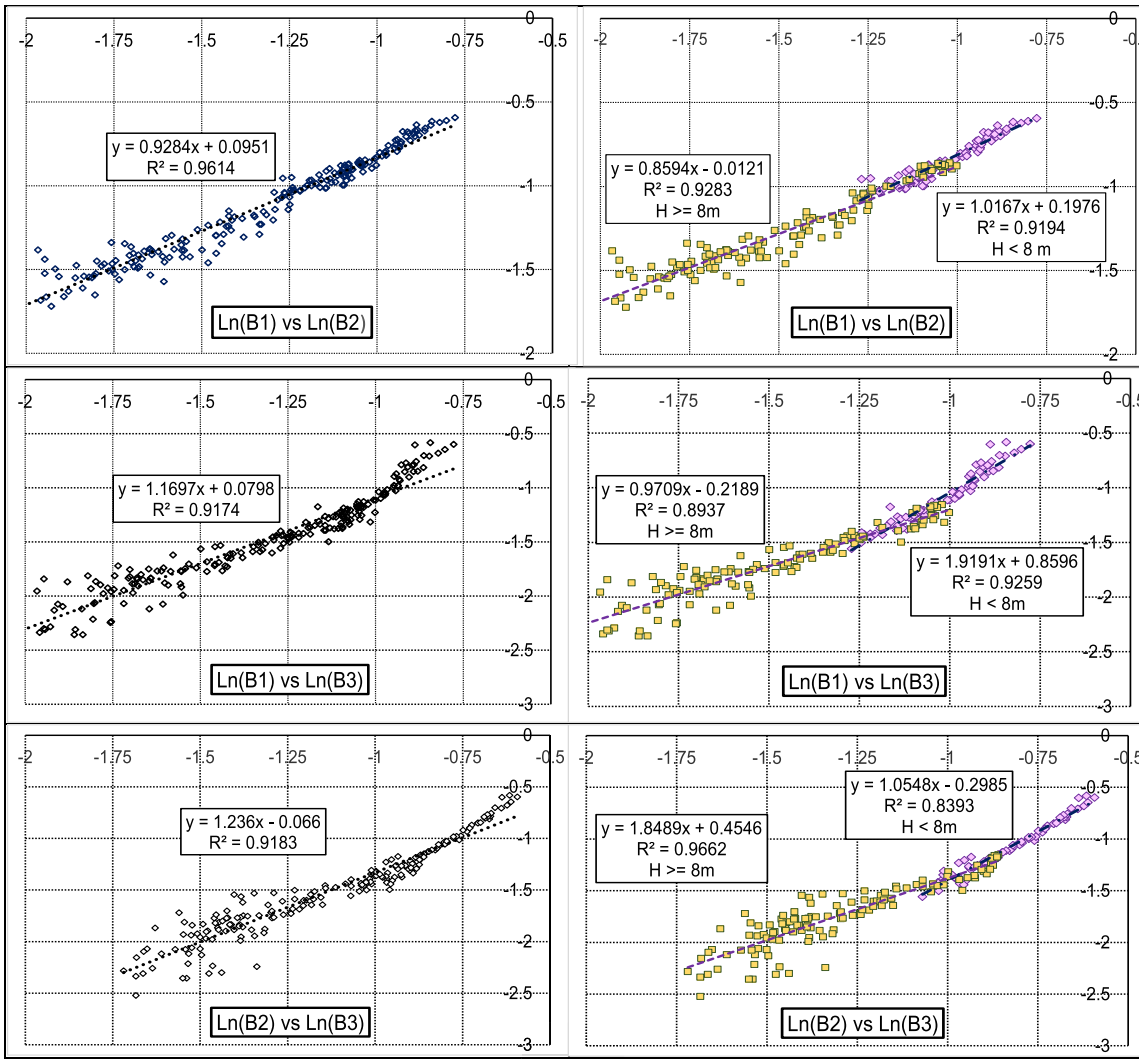

Figure 6. The attenuation coefficients ($Kd_{i,j}$ used for estimating $DII_{i,j}$ (left) and enhance DII (right) obtain from DII analysis in PlanetScope image date 28 June 2018

The dataset of attenuation coefficients regarding to DII algorithm (Lyzenga, 1981) will correspond to values of 0.9248; 1.1697 and 1.236, respectively. These coefficients adapt in whole depth range from 0 to 15 m. Processing equation systems of the Depth Invariance Indies (DIIs) according to Lyzenga's algorithm will be written.

$$\begin{cases} DII_{1,2} = Ln\left(Ref_{TOA,2} - Ref_{TOA,\infty,2}\right) - \left[0.9248 * \left(Ln\left(Ref_{TOA,1} - Ref_{TOA\infty,1}\right)\right)\right] \\ DII_{1,3} = Ln\left(Ref_{TOA,3} - Ref_{TOA,\infty,3}\right) - \left[1.1697 * \left(Ln\left(Ref_{TOA,1} - Ref_{TOA,\infty,1}\right)\right)\right] \\ DII_{2,3} = Ln\left(Ref_{TOA,3} - Ref_{TOA,\infty,3}\right) - \left[1.2360 * \left(Ln\left(Ref_{TOA,2} - Ref_{TOA,\infty,2}\right)\right)\right] \end{cases}$$

The dataset of attenuation coefficients regarding to enhanced DII algorithm (Tassan, 1996) will correspond to values of 1.0167; 1.9191 and 1.0548, respectively. These coefficients adapt in depth range from 0 to 8m. When the depth great than 8m, attenuation

coefficients of enhanced DII will be 0.8594; 0.9709 and 1.8489, respectively. Processing equation systems of enhanced Depth Invariance Indies (DIIs) according to Tassan's algorithm will be written more detail by

When H <= 8 m then

$$\begin{cases} DII_{1,2} = Ln\left(Ref_{TOA,2} - Ref_{TOA,\infty,2}\right) - \left[1.0167 * \left(Ln\left(Ref_{TOA,1} - Ref_{TOA,\infty,1}\right)\right)\right] \\ DII_{1,3} = Ln\left(Ref_{TOA,3} - Ref_{TOA,\infty,3}\right) - \left[1.9191 * \left(Ln\left(Ref_{TOA,1} - Ref_{TOA,\infty 1}\right)\right)\right] \\ DII_{2,3} = Ln\left(Ref_{TOA,3} - Ref_{TOA,\infty,3}\right) - \left[1.0548 * \left(Ln\left(Ref_{TOA,2} - Ref_{TOA,\infty,2}\right)\right)\right] \end{cases}$$

When H > 8m then

$$\begin{cases} DII_{1,2} = Ln\left(Ref_{TOA,2} - Ref_{TOA,\infty,2}\right) - \left[0.8594 * \left(Ln\left(Ref_{TOA,1} - Ref_{TOA,\infty,1}\right)\right)\right] \\ DII_{1,3} = Ln\left(Ref_{TOA,3} - Ref_{TOA,\infty,3}\right) - \left[0.9709 * \left(Ln\left(Ref_{TOA,1} - Ref_{TOA,\infty,1}\right)\right)\right] \\ DII_{2,3} = Ln\left(Ref_{TOA,3} - Ref_{TOA,\infty 3}\right) - \left[1.8489 * \left(Ln\left(Ref_{TOA,2} - Ref_{TOA,\infty,2}\right)\right)\right] \end{cases}$$

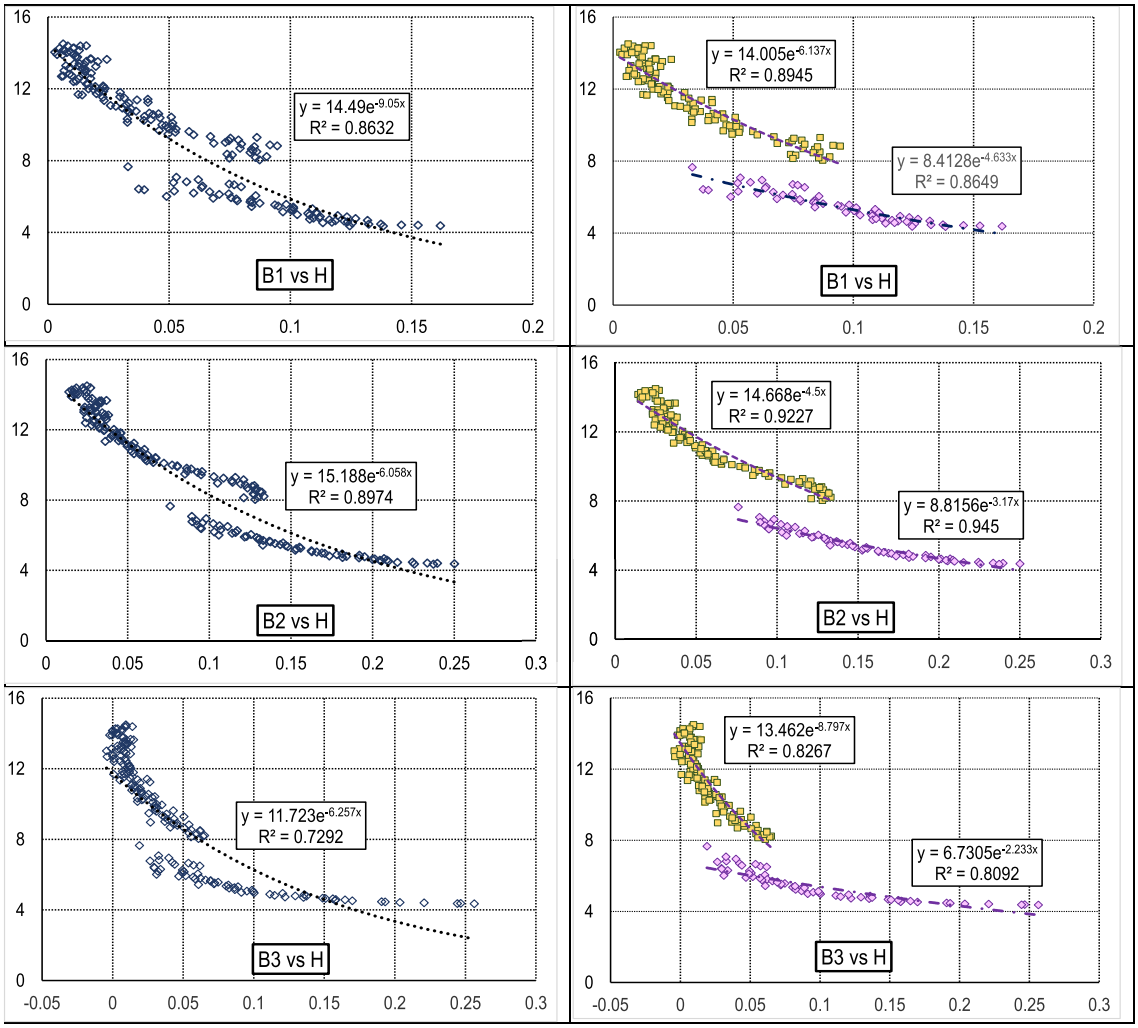

Figure 7. The attenuation coefficients Kd_i used for estimating BRI_i (left) and enhance BRI (right) obtain from BRI analysis in PlanetScope image date 28 June 2018

The dataset of attenuation coefficients regarding to BRI algorithm (Sagawa, 2010) will correspond to values of 9.05; 6.058 and 6.257, respectively. These coefficients adapt in whole depth range from 0 to 15 m. Processing equation systems of the Bottom Reflectance Indies (BRIs) according to Sagawa's algorithm will be written by

$$\begin{cases} \mathrm{BRI}_1 = e^{9.050}\left(\mathrm{Ref}_{\mathrm{TOA},1} - \mathrm{Ref}_{\mathrm{TOA},\infty,1}\right) \\ \mathrm{BRI}_2 = e^{6.058}\left(\mathrm{Ref}_{\mathrm{TOA},2} - \mathrm{Ref}_{\mathrm{TOA},\infty,2}\right) \\ \mathrm{BRI}_3 = e^{6.257}\left(\mathrm{Ref}_{\mathrm{TOA},3} - \mathrm{Ref}_{\mathrm{TOA},\infty,3}\right) \end{cases}$$

The dataset of attenuation coefficients regarding to enhanced BRI algorithm will correspond to values of 4.633; 3.17 and 2.233, respectively. These coefficients adapt in depth range from 0 to 8 m. When the depth great than 8 m, attenuation coefficients of enhanced BRI will be 6.137; 4.500 and 8.797, respectively. Processing equation systems of enhanced Bottom Reflectance Indies (BRIs) will be written more detail by

When H <= 8 m then

$$\begin{cases} \mathrm{BRI}_1 = e^{4.633}\left(\mathrm{Ref}_{\mathrm{TOA},1} - \mathrm{Ref}_{\mathrm{TOA},\infty,1}\right) \\ \mathrm{BRI}_2 = e^{3.170}\left(\mathrm{Ref}_{\mathrm{TOA},2} - \mathrm{Ref}_{\mathrm{TOA},\infty,2}\right) \\ \mathrm{BRI}_3 = e^{2.233}\left(\mathrm{Ref}_{\mathrm{TOA},3} - \mathrm{Ref}_{\mathrm{TOA},\infty,3}\right) \end{cases}$$

When H > 8 m then

$$\begin{cases} \mathrm{BRI}_1 = e^{6.137}\left(\mathrm{Ref}_{\mathrm{TOA},1} - \mathrm{Ref}_{\mathrm{TOA},\infty 1}\right) \\ \mathrm{BRI}_2 = e^{4.500}\left(\mathrm{Ref}_{\mathrm{TOA},2} - \mathrm{Ref}_{\mathrm{TOA},\infty,2}\right) \\ \mathrm{BRI}_3 = e^{8.797}\left(\mathrm{Ref}_{\mathrm{TOA},3} - \mathrm{Ref}_{\mathrm{TOA},\infty,3}\right) \end{cases}$$

Attentional, the subscripts of 1, 2, 3 correspond to Blue, Green and Red bands, respectively.

3.3.2. Extracting the distribution of SAV and other substrates by DII, BRI and their enhancements

(I) Distribution of SAV and others from DII algorithms

The DII, its enhanced images and more than 700 training points data were utilized to detect the SAVs and other substrates at An Chan coastal waters. There are 5 main objects were chosen to classify, as follow: (i) Seagrass (SG); (ii) Seaweed (SW); (iii) Rocky beds (RK); (iv) Sandy beds (SD); and (v) Others. Classification results of SAV canopies and other substrates in An Chan coastal waters obtained from DII, and enhanced DII images are shown in Fig. 8.

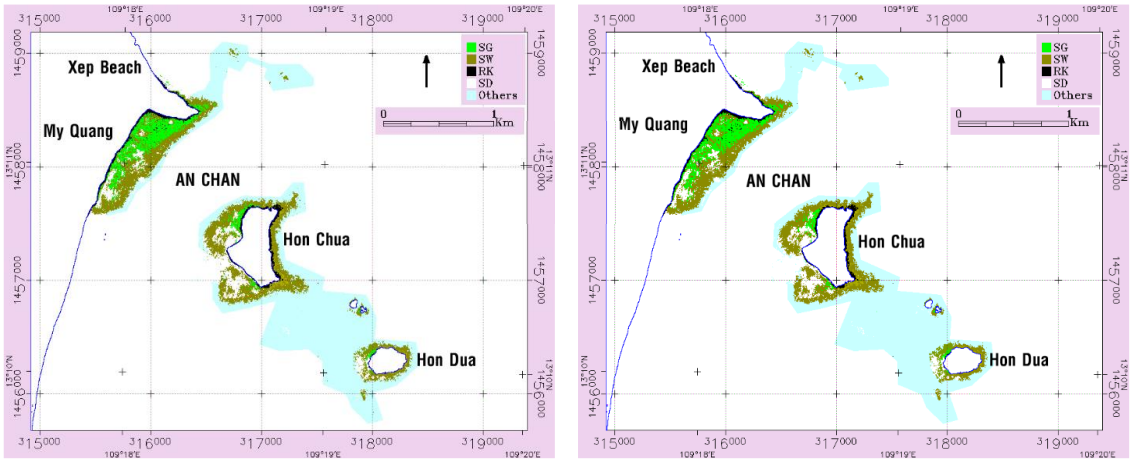

Figure 8. Distribution of submerge aquatic vegetation (SAV) canopies in An Chan-Hon Chua obtain from PS image (June-2018) base on Lyzenga's DII technique (left) and enhanced DII one (right)

(ii) Distribution of SAV and others from BRI algorithms

The BRI, its enhanced images and same training points data (as DII case) were also applied to detect the SAVs and other substrates at An Chan coastal waters. The

objects were chosen to classify are also similar, it mean (i) Seagrass (SG); (ii) Seaweed (SW); (iii) Rocky beds (RK); (iv) Sandy beds (SD); and (v) Others. Classification results of SAV canopies and other substrates in An Chan coastal waters obtained from BRI, and enhanced BRI images are shown in Fig. 9.

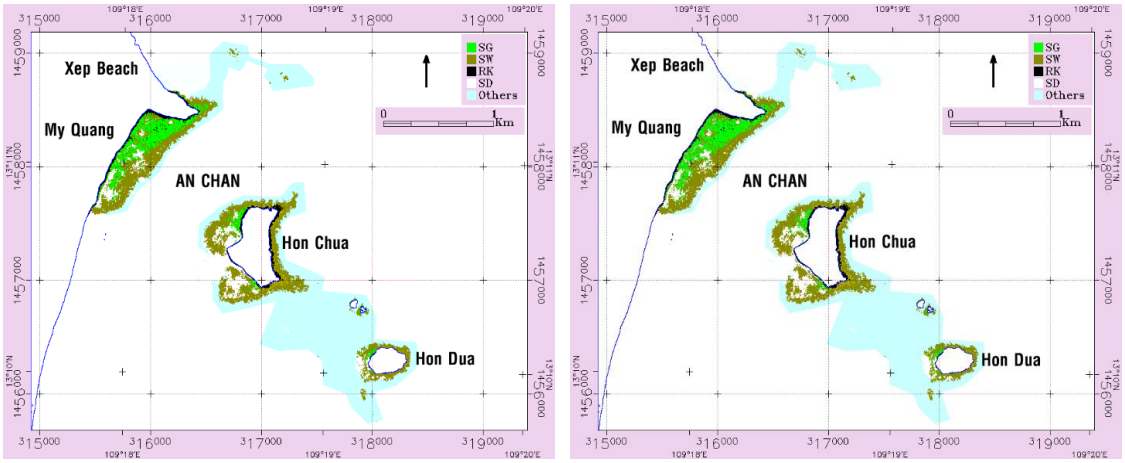

Figure 9. Distribution of submerge aquatic vegetation canopies in An Chan-Hon Chua obtain from PS image (June-2018) base on Sagawa's BRI technique (left) and enhanced BRI one (right)

(iii) Assessment the accuracy of SAV image classification by various processing techniques

The accuracies of SAV classification using different techniques are shown in Table 1, 2, 3 and 4. The overall accuracy and kappa coefficient of SAV classification by DII technique were 83.33% and 0.77, respectively. Whereas, the accuracy SAV classification by enhanced DII technique were 88.58 % and 0.84, respectively. The accuracy of SAV classification by BRI technique was 86.17 % and 0.81, respectively. The accuracy of SAV classification by enhanced BRI technique was 92.52 % and 0.90, respectively. Thus, the results of SAV classification by enhanced BRI technique provided the best accuracies and will be chosen for assessing the distribution of Submerge Aquatic Vegetation (SAV) canopies in An Chan coastal waters from PS satellite image.

Table 1. Confusion matrix of SAV classification results in An Chan coastal waters obtained from DII technique in Planetscope image, date 28 June 2018

Classes	SW	SG	RK	SD	Others	Sum
SW	60	61	29	9	1	160
SG	24	184	0	6	13	227
RK	23	1	1	46	0	71
SD	69	1	3	0	49	122
Others	0	5	0	0	130	135
Sum	176	252	33	61	193	715
Overall Accuracy		83.33 %				
Kappa coefficient		0.7733				

Table 2. Confusion matrix of SAV classification results in An Chan coastal waters obtained from enhanced DII technique in Planetscope image, date 28 June 2018

Classes	SW	SG	RK	SD	Others	Sum
SW	67	61	17	5	1	151
SG	8	195	0	6	9	218
RK	23	1	4	44	0	72
SD	86	1	3	0	49	139
Others	0	5	0	0	130	135
Sum	184	263	24	55	189	715
Overall Accuracy		88.58 %				
Kappa coefficient		0.8445				

Table 3. Confusion matrix of SAV classification results in An Chan coastal waters obtained from BRI technique in Planetscope image, date 28 June 2018

Classes	SW	SG	RK	SD	Others	Sum
SW	60	65	18	10	2	155
SG	20	196	0	1	15	232
RK	23	0	0	45	0	68
SD	69	2	2	0	53	126
Others	0	7	0	0	128	135
Sum	172	269	20	56	197	715
Overall Accuracy		86.17 %				
Kappa coefficient		0.8115				

Table 4. Confusion matrix of SAV classification results in An Chan coastal waters obtained from enhanced BRI technique in Planetscope image, date 28 June 2018

Classes	SW	SG	RK	SD	Others	Sum
SW	62	65	6	4	2	139
SG	5	206	0	1	9	221
RK	23	0	0	45	0	68
SD	95	1	2	0	53	151
Others	0	6	0	0	130	136
Sum	185	278	8	50	194	715
Overall Accuracy		92.52 %				
Kappa coefficient		0.8957				

3.3.3. The distributed areas of submerge aquatic vegetation (SAV) in An Chan coastal water from PS imageries

Classification results of SAV canopies and other substrates from PS satellite image base on enhanced BRI techniques, allow us to estimate distributed areas and their size.

The seagrass beds in My Quang is spread along the coast as a band with the width was approximately 180 to 320 m wide from the shoreline and its length was 1000 m long. The total seagrass area in My Quang was approximately 10.93 ha. Small seagrass patches also found in Hon Chua islet with a small patch was 0.94 ha in the NorthWest side and another was 0.24 ha in SouthWest. A very small patch of seagrass bed was approximately 0.11 ha also found in West Hon Dua islet. The total seagrass area in whole An Chan region (include My Quang-Hon Chua-Hon Dua) was approximately 12.22 ha.

The seaweed meadows in My Quang include scattered seaweed patches that lie interspersed with seagrasses on dead coral reefs with the distributed area of 4.25 ha and another patch was approximately 15.95 ha that located at the foot of the reefs in 3–4m

deep. The seaweed meadows in Hon Chua include broad patches of Sargassum lie around the islet and in the foot of the reef in 3–4 m deep with their width was 100 m wide and area were approximately 22.80 ha. The seaweed meadows in Hon Dua include broad patches of Sargassum lie around the islet and in the foot of the reef in 3–4 m deep with their width was about 50 m wide and area were approximately 5.72 ha. Besides, seaweed meadows also found in the underwater very small reef with the area was approximately 1.60 ha. The total seaweed area in whole An Chan region (include My Quang-Hon Chua-Hon Dua) was approximately 50.32 ha.

4. Conclusions

The distribution of submerge aquatic vegetation (SAV) canopies, include seagrass beds and seawed meadows in coastal waters of An Chan commune, Tuy An district, Phu Yen province can be detected very well by PlanetScope satellite image.

Thanks to data pre-processing by 2006 Lyzenga's algorithm, and the masking in PS image allow us to remove the signals of spectral noises from sun glint effect as well as other random noises.

Through of detail analysis of the water column correction by four different techniques (include their accuracy assessment after classification), we found enhanced BRI technique to provide the best accuracies with the overall accuracy and kappa coefficient of SAV classification were 92.52% and 0.90%, respectively. Enhanced BRI technique was chosen for assessment the distribution of Submerge Aquatic Vegetation (SAV) canopies in An Chan coastal waters from PS satellite image.

The total seagrass area in An Chan region was approximately 12.22 ha, with 10.93 ha seagrasses in My Quang, 1.18 ha in Hon Chua and 0.11 ha in Hon Dua.

The total seaweed area in An Chan region was approximately 50.32 ha, with 20.20 ha seaweed meadows in My Quang, 22.8 ha in Hon Chua, 5.72 ha in Hon Dua and a small part of 1.60 ha in underwater small reef.

Acknowledgments

The authors would like to thanks the staff of the Department of Natural Resources and Environment of Phu Yen province for their valuable support. This research was funded by the provincial project titled "Investigation, evaluation, the proposal of protected areas, and ecological landscape conservation in coastal waters of Phu Yen province (2016–2018)" and NAFOSTED under grant code 106.06-2017.305.

References

Bierwirth P., Lee T., Burne R., 1993. Shallow sea floor reflectance and water depth derived by unmixing multispectral imagery. Photogramm. Eng. Remote Sens., 59, 331–338.

Brando V.E., Anstee J.M., Wettle M., Dekker A.G., Phinn S.R., Roelfsema C., 2009. A physics based retrieval and quality assessment of bathymetry from suboptimal hyperspectral data. Remote Sens. Environ., 11, 755–770.

Brown C.J., Smith S.J., Lawton P., Anderson J.T., 2011. Benthic habitat mapping: A review of progress towards improved understanding of the spatial ecology of the seafloor using acoustic techniques. Estuarine, Coastal and Shelf Science, 92(3), 502–520.

Chauvaud S., Bouchon C., Maniere R., 1998. Remote sensing techniques adapted to high resolution mapping of tropical coastal marine ecosystems (coral reefs, seagrass beds and mangrove). International Journal of Remote Sensing, 19(18), 3625–3639.

Chen C.F., Va-Khin L., Ni-Bin C., Nguyen Thanh S., Phuoc Hoang Son T., Shou-Hao C., 2016. Multi-temporal change detection of seagrass beds using integrated Landsat TM/ETM +/OLI imageries in Cam Ranh Bay, Vietnam. Ecological Informatics, 35, 43–54.

Congalton R.G., 1991. A review of assessing the accuracy of classifications of remotely sensed data. Remote Sensing of Environment, 37(1), 35–46.

Conger C.L., Hochberg E.J., Fletcher C.H., Atkinson M.J., 2006. Decorrelating remote sensing color bands from bathymetry in optically shallow waters. IEEE Trans. Geosci. Remote Sens., 44, 1655–1660.

Department of Natural Resources and Environment of Phu Yen province (Phu Yen DONRE), 2014. Synthesis report of the project on building the system of information and materials on marine resources and environment in Phu Yen island , Phu Yen, Vietnam.

Hashim M., Nurul N.Y, Samsudin A., Komatsu T., Syarufuddin M., Nadzri R., 2014. Determination of seagrass biomass at Merambong Shoal in Straits of Johor using satellite remote sensing technique. Malayan Nature Journal, 66(1–2), 20–37.

Hedley J., Roelfsema C., Phinn S.R., 2009. Efficient radiative transfer model inversion for remote sensing applications. Remote Sens. Environ., 113, 2527–2532.

Ho H.P., 1969. Vietnamese seaweed; Learning Materials Center, Vietnam, 559p.

Klonowski W.M., Fearns P.R.C.S., Lynch M.J., 2007. Retrieving key benthic cover types and bathymetry from hyperspectral imagery. Journal of Applied Remote Sensing, 1, 011505.

Koedsin W., Wissarut I., Raymond J.R., Alfredo H., 2016. An Integrated Field and Remote Sensing Method for Mapping Seagrass Species, Cover, and Biomass in Southern Thailand. Remote Senings., 8, 292p. Doi:10.3390/rs8040292.

Gašparović M., Medak D., Pilaš I., Jurjević L., Balenović I., 2018. Fusion of sentinel-2 and planetscope imagery for vegetation detection and monitoring. Int. Arch. Photogramm. Remote Sens. Spatial Inf. Sci., XLII-1, 155–160, https://doi.org/10.5194/isprs-archives-XLII-1-155-2018.

Green E.P., Mumby P.J., Edwards A.J., Clark C.D., 1996. A review of remote sensing for the assessment and management of tropical coastal resources. Coastal Management, 24(1), 1–40.

Larkum W.L., Dekker A., Brando V., Anstee J., Fyfe S., Malthus T., Karpouzli E., 2006. Remote Sensing of Seagrass Ecosystems: Use of Spaceborne and Airborne Sensors Seagrasses: Biology, Ecology and Conservation, Springer Netherlands, 347–359.

Le C.Y.L., Zha Y., Sun D., Huang C., Zhang H., 2011. Remote estimation of chlorophyll a in optically complex waters based on optical classification. Remote Sensing of Environment, 115(2), 725–737.

Lee Z.P., Carder K.L, Arnone R.A., 2002. Deriving inherent optical properties from water color: A multi-band quasi-analytical algorithm for optically deep waters, Applied Optics, 41, 5755–5772.

Lyzenga D.R., 1981. Remote sensing of bottom reflectance and water attenuation parameters in shallow water using aircraft and Landsat data. Int. J. Remote Sens., 2, 71–82.

Lyzenga D.R., Malinas N.P., Tanis F.J., 2006. Multispectral bathymetry using a simple physically based algorithm. IEEE Trans. Geosci. Remote Sens., 44, 2251–2259.

Mobley C.D., Sundman L.K., Davis C.O., Bowles J.H., Downes T.V., Leathers R.A., Montes M.J., Bissett W.P., Kohler D.D.R., Reid R.P., 2005. Interpretation of hyperspectral remote-sensing imagery by spectrum matching and Look-Up Tables. Appl. Opt., 44, 3576–3592.

Mumby P.J., Clark C.D., Green E.P., Edwards A.J., 1998. Benefits of water column correction and contextual editing for mapping coral reefs. Int. J. Remote Sens., 19, 203–210.

Mumby P.J., Edwards A.J., Clark C.D., 1999. The cost-effectiveness of remote sensing for tropical coastal resources assessment and management. Journal of Environmental Management, 55, 157–166.

Phillips R., Mennez C.E.G., 1998. Seagrasses. Publication of Smithsonian institution: Washington D.C., 34, 105p.

Pu R., Bell S., Meyer C., Lesley B., Zhao Y., 2012. Mapping and assessing seagrass along the western coast of Florida using Landsat TM and EO-1 ALI/Hyperion imagery. Estuarine, Coastal and Shelf Science, 115, 234–245.

Pu R., Bell S., 2017. Mapping seagrass coverage and spatial patterns with high spatial resolution IKONOS imagery. International Journal of Applied Earth Observation and Geoinformation, 54, 145–158.

Purkis S.J., Pasterkamp R., 2004. Integrating in situ reef-top reflectance spectra with LANDSAT TM imagery to aid shallow-tropical benthic habitat mapping. Coral Reefs, 23, 5–20.

Sagawa T., Boisnier E., Komatsu T., Mustapha K.B., Hattour A., Kosaka N., Miyazaki A., 2010. Using bottom surface reflectance to map coastal marine areas: A new application method for Lyzenga's model. Int. J. Remote Sens., 31, 3051–3064.

Siregar V.P, Agus S.B., Subarno T., Prabowo N.W., 2017. Mapping shallow waters habitats using OBIA by applying several approaches of depth invariant index in North Kepulauan Seribu, 2016. IOP Conf. Series: Earth and Environmental Science, 149, 012052.

Spitzer D., Dirks R., 1987. Bottom influence on the reflectance of the sea. Int. J. Remote Sens, 8, 279–290.

Tassan S., 1996. Modified Lyzenga's method for macroalgae detection in water with non-uniform composition. Int. J. Remote Sens., 17, 1601–1607.

Tien V.N., 2013. Resource of seagrass beds in Vietnam; Publisher of Natural Science and Technology: Hanoi, 346p.

Tsutsui I., Nang Q.H., Dinh H.N., Arai S., Yoshida T., 2005. The common marine plants of southern Vietnam; Japan Seaweed Association: Kochi, Japan, 250p.

Vietnam Red Book, Part II: Plants, 2007. Science and Technology Publishing House: Hanoi, Vietnam.

Yang C., Yang D., Cao W., Zhao J., Wang G., Sun Z., Xu Z., Ravi K.M.S., 2010. Analysis of seagrass reflectivity by using a water column correction algorithm. Int. J. Remote Sens, 31, 4595–4608.

http://www.algaebase.org/.